Journal of Zhejiang University-SCIENCE B (Biomedicine & Biotechnology) *2023 24(10):922-934*
www.jzus.zju.edu.cn; www.springer.com/journal/11585
E-mail: jzus_b@zju.edu.cn

Research Article
https://doi.org/10.1631/jzus.B23d0003

Cellulose nanofibril matrix drives the dynamic formation of spheroids

Yi LU[1,2,3*], Guo LI[1,2*], Yeqiu LI[2], Yuan YAO[1,2,3✉]

[1]*College of Chemical and Biological Engineering, Zhejiang University, Hangzhou 310027, China*
[2]*ZJU-Hangzhou Global Scientific and Technological Innovation Center, Zhejiang University, Hangzhou 311215, China*
[3]*School of Physical Science and Technology, ShanghaiTech University, Shanghai 201210, China*

Abstract: Multicellular spheroids, which mimic the natural organ counterparts, allow the prospect of drug screening and regenerative medicine. However, their application is hampered by low processing efficiency or limited scale. This study introduces an efficient method to drive rapid multicellular spheroid formation by a cellulose nanofibril matrix. This matrix enables the facilitated growth of spheroids (within 48 h) through multiple cell assembly into size-controllable aggregates with well-organized physiological microstructure. The efficiency, dimension, and conformation of the as-formed spheroids depend on the concentration of extracellular nanofibrils, the number of assembled cells, and the heterogeneity of cell types. The above strategy allows the robust formation mechanism of compacted tumoroids and hepatocyte spheroids.

Key words: Cellulose; Nanofibril; Matrix; Self-assembly; Spheroid

1 Introduction

The assembly of spatially ordered multiple cells as spheroids or tumoroids is a promising avenue for tissue engineering and personalized medicine (Steinberg, 1962; Gonzalez-Rodriguez et al., 2012; Tevis et al., 2017; Tuveson and Clevers, 2019; Chen et al., 2023). Researchers require models to replicate the multicellular nature and three-dimensional (3D) stromal environment in an in vivo tumor (Tevis et al., 2017). Biomacromolecules from the extracellular matrix (ECM) are critical to connect the material surfaces and living tissues. These ECM biomacromolecules with specific topology as nanofibril or network between the material–organism interface are essential for organogenesis (Ren et al., 2019) and play a significant role in remodeling the surrounding tumor microenvironment (Yeatts et al., 2013; Huang et al., 2015). Thus, ECM nanofibrils or networks can modulate cellular fate or reorganize the tissue architecture or even change the progression of cancer metastasis. For example, the osteochondral interface for bone development undergoes nanofibril gradual transitions by the shifting of cell number, density, polarization, orientation, and nanofibril arrangement along the osteochondral interface (Kronenberg, 2003; Jadin et al., 2005; Ren et al., 2016). In pathological contexts, the ECM nanofibril can undergo remodeling (Goetz et al., 2011; Martinez-Vidal et al., 2021), which is a progressive transition to ECM anisotropy that occurs in many cancers (Mouw et al., 2014; Park et al., 2020; Martinez-Vidal et al., 2021; di Martino et al., 2022).

Spheroids or tumoroids as multicellular aggregates embedded in an ECM are a prevalent model to mimic the natural microenvironment. The bottom-up assembly of a spatially ordered aggregate made from multiple cells based on the assembly principle is a highly promising strategy for tissue engineering (Mueller et al., 2020; Rasoulinejad et al., 2020). Over the last decade, artificial materials acting as the ECM have facilitated multiple-cell aggregation, organization, differentiation, and functionalization (Malafaya et al., 2007; Chen et al., 2017; Hale et al., 2018; Landry et al., 2018; Ortega-Prieto et al., 2018; Rossi et al., 2018; Alegret et al.,

✉ Yuan YAO, yyao1@zju.edu.cn
* The two authors contributed equally to this work
Yuan YAO, https://orcid.org/0000-0001-5262-5115

Received Mar. 16, 2023; Revision accepted May 8, 2023;
Crosschecked July 19, 2023

2019; Grassi et al., 2019; Roi et al., 2019). Spheroid formation requires multiple-cell assembly based on a scaffold matrix for mechanical support or biochemical signals (Edelman, 1983; Hegedüs et al., 2006). Artificial scaffold matrices for 3D culture systems can be derived from natural compounds to synthetic polymers. For example, decellularized matrix, electrospun nanofiber, hydrogel functionalized with peptides, or polymer-based macroporous scaffolds have been investigated for their varying functions in facilitating spheroid formation (Sun et al., 2007; Mohan et al., 2014; Louis et al., 2017; Jaeckel et al., 2018; Roerink et al., 2018; Rossi et al., 2018; Grassi et al., 2019). The as-formed units usually have a representative microstructure and biological function to their actual tissue counterparts (Steinberg, 1962; Gonzalez-Rodriguez et al., 2012; Tuveson and Clevers, 2019). The artificial ECM in 3D culture systems, ranging from natural derivatives to synthetic polymers (Jaeckel et al., 2018; Roerink et al., 2018; Rossi et al., 2018; Grassi et al., 2019), provides a spatial scaffold as mechanical support (Amaral and Pasparakis, 2016; Drost and Clevers, 2018; Rossi et al., 2018). However, improving the processing efficiency (assembly time, spheroid dimension) and experimental throughput remains a challenge, as does the fabrication reproducibility, and scale-up capacity of such materials (Lawlor et al., 2021).

Bioengineering tools and diversified nanomaterials modify the aggregating microenvironment for more efficient cell assembly (Bagley et al., 2017; Broutier et al., 2017; Cruz et al., 2017; Bergmann et al., 2018; Jager et al., 2018; Karzbrun et al., 2018; Qian et al., 2018; Bryant et al., 2019; Garreta et al., 2019; Homan et al., 2019; Miller et al., 2019; Phipson et al., 2019; Li et al., 2021). Biocompatible, long, flexible cellulose nanofibrils (CNFs) have been applied as biomaterials in tissue engineering as scaffolds (Mittal et al., 2018; Ferreira et al., 2020; Krüger et al., 2020; Yang et al., 2020; Zhang et al., 2020; Curvello et al., 2021; Evdokimova et al., 2021), and have been increasingly popular in preparing functional scaffolds due to being cost-effective and straightforward (Mittal et al., 2018; Ferreira et al., 2020; Yang et al., 2020; Zhang et al., 2020). Nanocellulose-based biomaterials such as foams and aerogels can be synthesized effortlessly using green, scalable approaches (Karageorgiou and Kaplan, 2005; Abdul Khalil et al., 2014; Hu et al., 2014; Al-Qararah et al., 2015; Martoïa et al., 2016; Nechyporchuk et al., 2016a, 2016b; Reid et al., 2017; Mittal et al., 2018; Ferreira et al., 2020; Yang et al., 2020; Zhang et al., 2020). The biocompatibility and physicochemical properties of CNFs make them a promising candidate for biomedical engineering (Park et al., 2015; Thunberg et al., 2015; Abouzeid et al., 2018; Krüger et al., 2020; Curvello et al., 2021). Herein, we developed an effective CNF-driven method to facilitate spheroid formation. The strategy of CNF matrix-driven formation of spheroid (CMDO) involves the use of CNFs as a matrix quantitatively integrated into multiple cells. We validated this method in multiple cell types (including cancer cell lines, fibroblast cells, and hepatocytes). The as-fabricated tumoroid or spheroid represents the replication of the physiological structure of the actual tissue counterpart.

2 Materials and methods

2.1 Cellulose nanofibril preparation

Never-dried sulfite softwood pulp (10 g) with a hemicellulose content of 13.8% (mass fraction) and lignin content of 0.7% (mass fraction) (Nordic Paper, Sweden) was placed into a three-necked round-bottom flask at a pulp concentration of 1.0% (mass fraction). Subsequently, 156 mg of 2,2,6,6-tetramethylpiperidine-1-oxyl (TEMPO; Sigma-Aldrich, Shanghai, China) and 1028 mg of sodium bromide (NaBr; Sigma-Aldrich) were added to the pulp, followed by mixing. Then, 30 mL of 14% (0.14 g/mL) NaClO solution (VWR International, Shanghai, China) was added to the mixture dropwise under stirring. Further oxidization of the pulp was conducted with 1% (10 g/L) $NaClO_2$ in acetate buffer at pH=4.8 for 48 h. Following oxidation, the fibers were thoroughly washed with distilled water and disintegrated by passing through a microfluidizer. Finally, a CNF solution with a concentration of about 0.7% (7 g/L) and a charge density of 1476 μEq/g was obtained.

2.2 Atomic force microscopy characterization

The surface charge density of CNFs was measured by polyelectrolyte titration at pH=9, with a poly (diallyldimethylammonium chloride) (PDADMAC) solution. The topologic structures were assessed using a dimension ICON atomic force microscopy (AFM) fast scanning system (Bruker, Germany) set to tapping mode.

2.3 Cell culture

MDA-MB-231, A549, Min6, tail-tip fibroblast (TTF), and L929 cells were obtained from the Chinese Academy of Sciences (Shanghai, China). A pancreatic cancer cell line was obtained from a xenograft mouse cell. All cell lines were maintained in Dulbecco's modified Eagle medium (DMEM) with 10% (mass fraction) fetal bovine serum (FBS) and 1× penicillin/streptomycin (100 mg/L). Mouse hepatocytes were cultured in previously reported medium (Katsuda et al., 2017). Cell viability was examined by cell counting kit-8 (Dojindo, Japan).

2.4 Mass spectrometry

Tandem mass tag (TMT) labeling: freshly prepared cell pellets were lysed using 8 mol/L urea in 100 mol/L of Tris-HCl at pH=8.5. The protein concentration was measured by the bicinchoninic acid (BCA) assay (Pierce, Rockford, IL, USA), wherein 100 μg of each sample was transferred to a new tube for reduction and alkylation with Tris(2-carboxyethyl)phosphine and iodoacetamide, respectively. We took an equal amount of peptide for TMT labeling based on the peptide concentration by following the manufacturer's protocol (Thermo Fisher Scientific, Waltham, MA, USA). The desalted peptide was analyzed using modified MudPIT separation. The sample mixture was analyzed on an Easy-nLC1000 chromatograph (Thermo Scientific, Waltham, MA, USA).

2.5 Quantitative proteomics

Tandem mass spectrometry (MS/MS) analysis was performed by an Orbitrap Elite ETD mass spectrometer (Thermo Scientific) equipped with a nano-electrospray ionization source using distal 2-kV spray voltage. The full-scan resolution was set to 60 000 and MS/MS scan resolution was set to 30 000.

2.6 Bioinformatics analysis

Protein identification and quantification were conducted with the Integrated Proteomics Pipeline (IP2; http://integratedproteomics.com). MS/MS spectra were applied against a Swiss-Prot *Homo sapiens* database using ProLuCID and DTASelect2.0. The differentially expressed lists were subjected to Ingenuity Pathway Analysis (IPA; Qiagen, Ingenuity Systems) and STRING (https://cn.string-db.org) for biological canonical pathway, function, and network analyses. These analyses were performed herein as proof-of-knowledge to help classify, model, analyze, and understand complex biological and chemical systems.

2.7 Dimension measurement of spheroid

Images of CMDOs were captured by a Motic stereoscope (BM2000, 4X, Motic, Xiamen, China) with six replicates for each sample and processed by CellProfiler (https://cellprofiler.org) using a customized pipeline. The measurement unit of MaximumRadius was the size of the spheroid.

2.8 qPCR

The total RNA of target cells was isolated with TRIzol Reagent (Invitrogen, USA), and quantitative PCR (qPCR) was performed with SYBR® Premix Ex Taq™ II with ROX (TaKaRa, Beijing, China) on a StepOnePlus™ PCR System (Thermo Fisher Scientific, Waltham, MA, USA). The primer sequences are listed in Table 1.

2.9 Histology and immunohistochemistry

All samples were fixed in 4% (0.04 g/mL) paraformaldehyde by standard protocols. The fixed samples were stained with hematoxylin and eosin (H&E) for histopathological evaluation, and the images were processed with Leica THUNDER Imager (Leica, Germany).

2.10 Statistical analysis

Statistical differences were assessed using an unpaired Student's *t*-test by GraphPad Prism software. The significance levels were set at * $P<0.05$, ** $P<0.01$, and *** $P<0.001$, whereas $P>0.05$ was considered as not significant.

3 Results and discussion

3.1 CMDOs

In the CMDO system, CNFs (Fig. S1) were prepared as the biomimetic ECM. They were fabricated by following a previous report (Kobayashi et al., 2014), which yielded individual nanofibrils with a coniferous shape of 20–30 nm in width and 300–500 nm in length (Fig. 1). The properties of these CNFs are suitable for spheroid formation. CNFs are low-cost and biocompatible, with good performance on cell viability (Mittal et al., 2018; Ferreira et al., 2020; Yang

Table 1 Primer sequences for quantitative PCR (qPCR)

Gene	Primers (5'→3')
Alpha fetoprotein (*Afp*)	F: CTTCCCTCATCCTCCTGCTAC
	R: ACAAACTGGGTAAAGGTGATGG
Albumin (*Alb*)	F: TGCTTTTTCCAGGGGTGTGTT
	R: TTACTTCCTGCACTAATTTGGCA
Hepatocyte nuclear factor 4 α (*Hnf4α*)	F: CACGCGGAGGTCAAGCTAC
	R: CCCAGAGATGGGAGAGGTGAT
Cytochrome P450, family 3, subfamily A, polypeptide 11 (*Cyp3a11*)	F: TGGTCAAACGCCTCTCCTTGCTG
	R: ACTGGGCCAAAATCCCGCCG
Keratin 19 (*Krt19*)	F: GGGGGTTCAGTACGCATTGG
	R: GAGGACGAGGTCACGAAGC
T-box transcription factor 3 (*Tbx3*)	F: GAGGCCAAGGAACTTTGGGA
	R: AGGGAACATTCGCCTTCCTG
Sex-determining region Y-box 9 (*Sox9*)	F: TGCTGGTGTGGTGAAAGGTT
	R: CCAGGAGCAACAAAGTTGGC
β-Actin	F: GGCTGTATTCCCCTCCATCG
	R: CCAGTTGGTAACAATGCCATGT

F: forward; R: reverse.

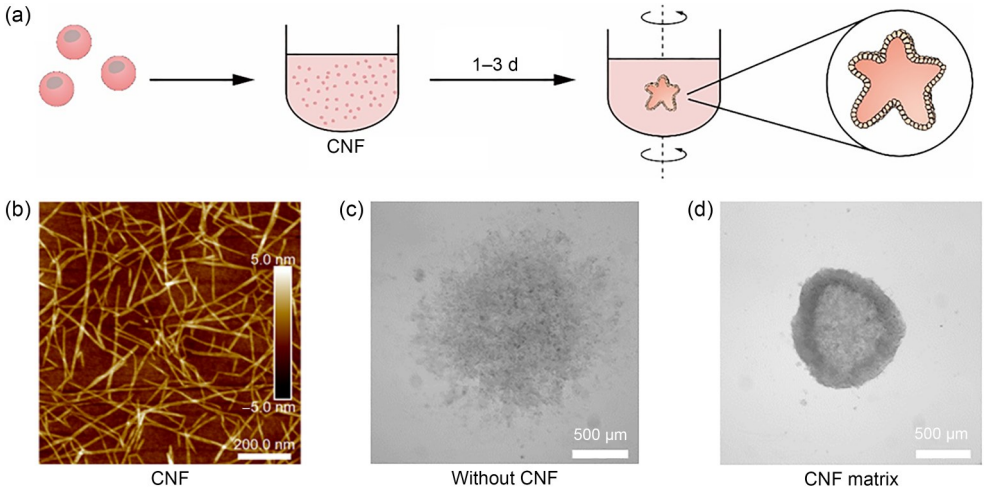

Fig. 1 Cellulose nanofibril (CNF) matrix-driven formation of spheroids (CMDO). (a) The strategy of CMDO. (b) Atomic force microscopy (AFM) images of CNFs at a gradient concentration of 0.76 μg/mL. (c) Pancreatic cancer cell aggregate without CNFs (48 h). (d) Pancreatic cancer cell spheroid formation (48 h).

et al., 2020; Zhang et al., 2020). The length/width dimension of as-fabricated CNFs is similar to the size of natural collagen nanofibrils (Winkler and Kaplan, 2001; Robins, 2006; Davies, 2013; Fang et al., 2013; Holmes et al., 2018), allowing the construction of a biomimetic microenvironment. In living tissues, cells exist in complex microenvironments, with cells in a 3D niche and interacting with the ECM. Hence, the flexible CNFs, based on their biomimetic nanostructure, should allow fast multi-cell aggregation for CMDO. The spheroid was achieved within 48 h (Fig. 1), with a significant improvement in processing efficiency compared to cells grown in Matrigel, with the latter taking 1–3 weeks and yielding small cell clusters (Badea et al., 2019; Xiao et al., 2022). Thus, it was confirmed that CNFs are required for spheroid formation because the control group without CNF failed to form a whole unit.

Furthermore, it was observed that the formation of tumoroid was dependent on CNF concentration (Fig. S2). To this end, a concentration of 0.38–0.76 μg/mL of CNFs was the optimal range for the formation of

spheroids, to efficiently drive cell assembly into a single, integrated unit (Fig. S2). CNFs at lower concentrations (0–0.12 μg/mL) only formed small clusters sparsely dispersed in culture media (Fig. S2). Thus, by tuning the CNF concentration, the fabrication of CMDOs is controllable: the clustered or dispersed cells are assembled into aggregates with pre-set dimensions. To better understand the formation process, fluorescence images were used to explore the aggregation process for 24 h (Fig. 2a). H&E staining allowed the assessment of microstructure of the formed spheroids (Figs. 2b and 2c), which showed that spheroids were found in a mesostructured space surrounded by ring-shaped condensate cells (Fujii et al., 2016; Saito et al., 2019; Lawlor et al., 2021).

3.2 Quantitative proteomics for tumoroids

In order to understand the protein–protein interactions during spheroid formation, we conducted quantitative proteomics. Changes in protein expression occurring within the spheroid initiation phase (0–24 h) might be vital in developing this complex tumor-like structure. However, the molecular mechanisms involved in the onset of tumoroid remain elusive. We performed systematic quantitative proteomics involving TMT labeling, which allowed the simultaneous identification and quantification of the protein expression profile.

The proteomic trajectories implicated in molecular mechanisms relevant to cell death and survival, cellular development, cellular growth, and proliferation were observed at 8 h. The proteomics profile transformed into cancer pathogenesis, cellular movement, or tissue development at 24–48 h (Fig. S3). These protein expression changes corresponded with the physiological features of the aggregating process at 8 h and the stabilized stage at 24–48 h (Fig. S3). Numerous metabolic processes participated in epithelial cell development, cell junction organization, assembly, and related functions. Most of the identified proteins were classified into cell adhesion, movement, and communication, which was a response to the microenvironmental change (Fig. 3b). The heatmap showed the proteomic profile during aggregation (Fig. S3), and two enrichments during epithelial cell development (Fig. S4) and cell adhesion and movement (Fig. S5) were also clearly illustrated. The enhancement of laminin (Fig. 3a) indicated cell movement and cell–cell communication, which was in good agreement with the results of IPA analysis (Fig. 3b)

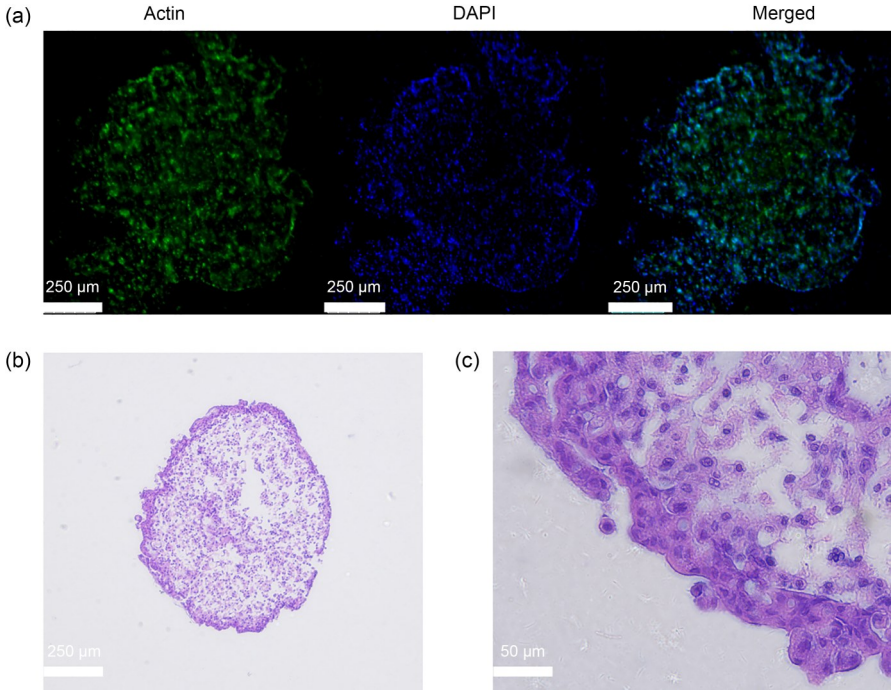

Fig. 2 Microscopic images of spheroids. (a) Immunostaining of aggregated spheroids with 0.38 μg/mL cellulose nanofibril (CNFs) at 24 h: actin staining (green), DAPI (blue), and merged image. (b, c) H&E staining of pancreatic cancer cell spheroids with 0.38 μg/mL CNFs at 48 h. DAPI: 4',6-diamidino-2-phenylindole; H&E: hematoxylin and eosin.

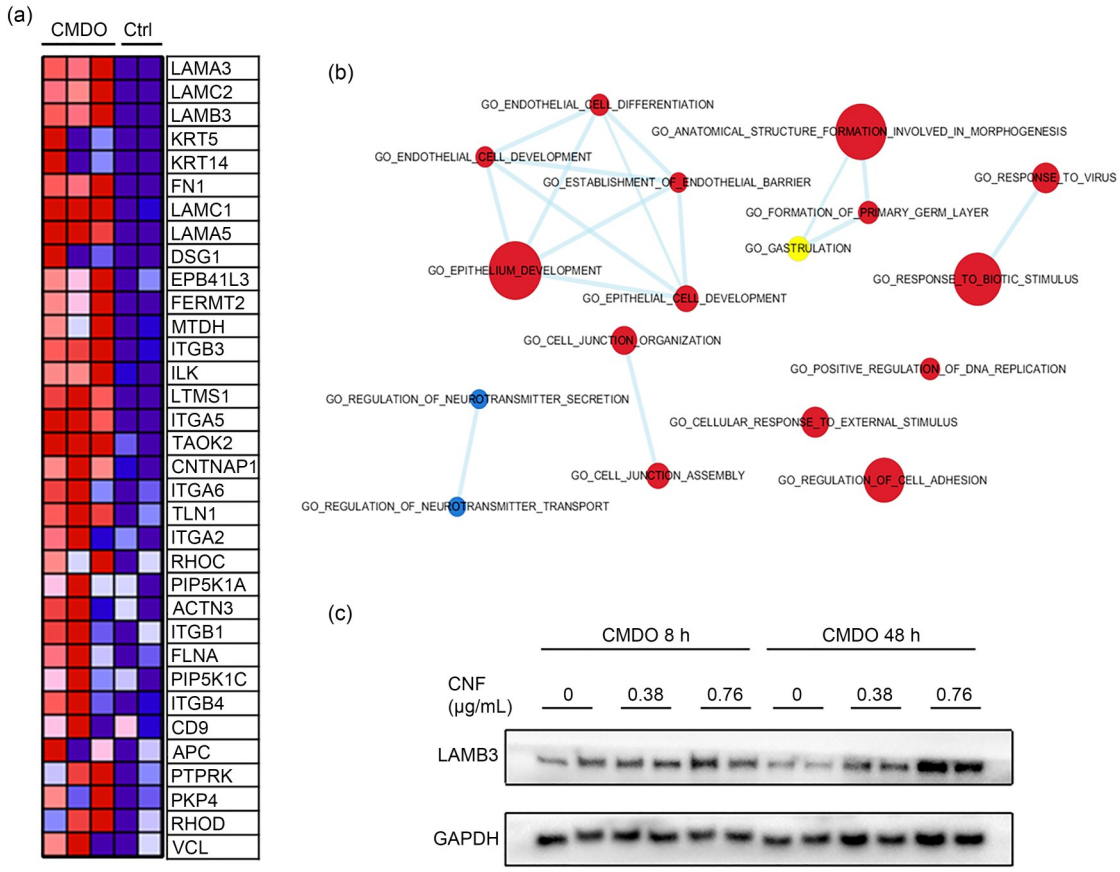

Fig. 3 Quantitative proteomics for tumoroids. (a) Heatmap of proteins related to cell junction and assembly during tumoroid formation (red represents upregulation while blue represents downregulation). (b) Ingenuity Pathway Analysis (IPA) protein function clusters based on quantitative proteomics (red represents upregulation, blue represents downregulation, and yellow represents no variation). (c) Western blot of laminin subunit β3 (LAMB3) at different cellulose nanofibril (CNF) gradients, with glyceraldehyde 3-phosphate dehydrogenase (GAPDH) acting as control. CMDO: CNF matrix-driven formation of spheroids; Ctrl: control.

and protein–protein networks on STRING (Fig. S6). Laminin is a protein present in the ECM of organs or tissues, providing support and attachment for cells (Aumailley, 2013). Together with other ECM proteins, laminin molecules form sheets and drive the cells to establish connective tissue (Miner and Yurchenco, 2004; Nguyen and Senior, 2006; Rohn et al., 2018). Furthermore, *LAMB3*, encoding the laminin subunit β3 protein, regulates cell movement and attachment (Fitsialos et al., 2008; Chung et al., 2014; Jung et al., 2018; Zhu et al., 2020) and is directly involved in the formation and organization of basement membranes during morphogenesis (Buchroithner et al., 2004; Fitsialos et al., 2008; Chung et al., 2014). Therefore, we validated its expression profile by western blot (Fig. 3c) and found it to be highly promoted during tumoroid formation.

3.3 Reproducibility of CMDO

We next assessed the reproducibility of CMDO on 96-well plates. With a given number of initiating cells and dosage of CNFs, the reproducibility of CMDO was high as shown by six repeats for each CNF concentration at 48 h (Fig. 4a). Furthermore, the stabilization of CMDO was achieved within 2 d, indicating significant improvement in processing efficiency compared with control groups without CNF. Additionally, the resulting tumoroid showed morphological homogeneity (Fig. 4a). Cell viability and dimension accuracy were reproducible across all 96 wells (Figs. 4b and 4c).

3.4 Application by CMDO on different cell types

We further evaluated the performance of CMDO using different cell types, including cancer cell lines

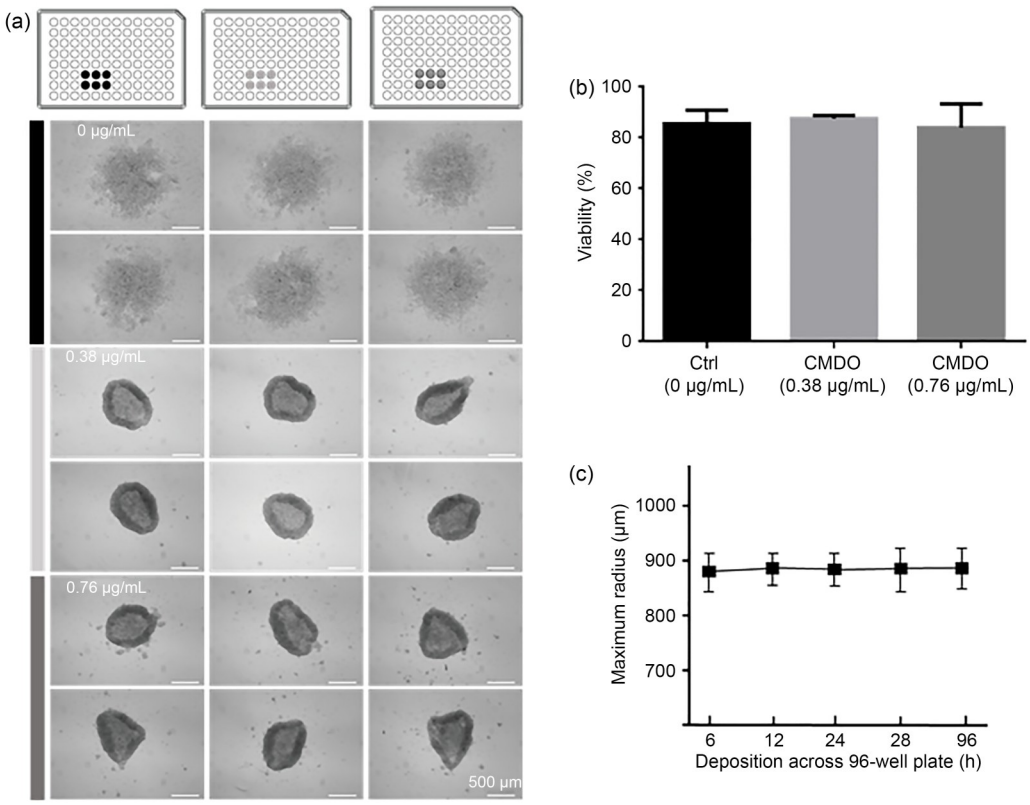

Fig. 4 Experimental reproducibility of CMDO. (a) Experimental reproducibility of pancreatic cancer cell spheroids on 96-well plates. The reproducibility was high, as evidenced by six repeats for each cellulose nanofibril (CNF) concentration. (b) Viability of cells with different concentrations of CNF. (c) The dimension of spheroids (measured by maximum radius) within the 96-well plate. Data are expressed as mean±standard deviation (SD), *n*=6. CMDO: CNF matrix-driven formation of spheroids; Ctrl: control.

(A549 and MDA-MB-231), fibroblast cell line (L929), TTF, β-cells (Min6), and mouse hepatocyte (HMM). A larger number of cells were found to generate greater-sized spheroids (Figs. 5a–5f). The experimental reproducibility was high but with a slight standard deviation. Thus, CNFs were regarded as useful as a universal biomimetic scaffold that dynamically facilitates cell aggregation and spheroid formation (Figs. 5b–5f). The cell type was detected to determine the shape, conformation, and dimension of the as-formed spheroid. Cancer cells all exhibited a spheroidal morphology, whereas Min6 exhibited a polygonal shape (Fig. 5g). Spheroids grown from L929 cells showed a typical round conformation, while TTF presented a condensation architecture (Fig. 5g).

3.5 Hepatocyte spheroid by CMDO

Hepatocytes are the main components and functional cells of the liver (Katsuda et al., 2017). Herein, we constructed a hepatocyte spheroid by CMDO. CNFs were able to drive mouse hepatocytes into a spheroid with excellent reproducibility (Fig. S7). An integrated and stable hepatocyte spheroid array with hepatic function is in high demand for clinical research and the pharmaceutical industry. Thus, we built a high-throughput hepatocyte array, wherein liver spheroids were formed in unified and controlled dimensions. For each hepatocyte spheroid, the hepatic function was validated by functional gene expression (Fig. 6). The expression of functional liver markers was significantly increased (hepatocyte markers: albumin (*Alb*), hepatocyte nuclear factor 4 α (*Hnf4α*), and cytochrome P450, family 3, subfamily A, polypeptide 11 (*Cyp3a11*); cholangiocyte marker: keratin 19 (*Krt19*)), suggesting parallel lineage specification into hepatocytes and polarized cholangiocytes (Fig. 6). Furthermore, the hepatocyte spheroids exhibited higher expression of liver stem cell markers, such as alpha fetoprotein (*Afp*), T-box transcription factor 3 (*Tbx3*), and sex determining region Y-box 9 (*Sox9*).

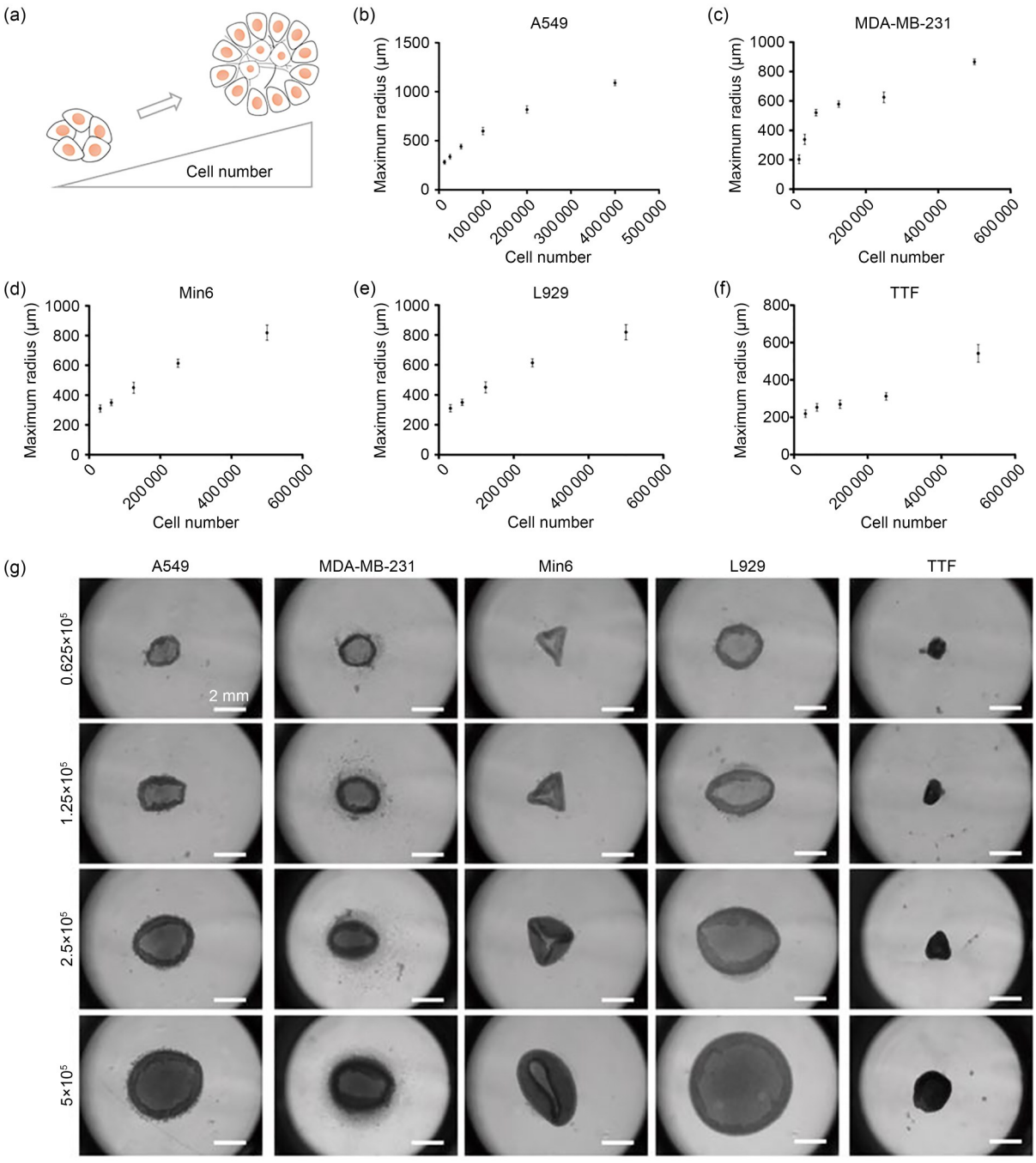

Fig. 5 Cellulose nanofibril (CNF)-induced spheroid formation at 48 h with increasing cell numbers. (a) Illustration of the relationship between spheroid dimension and cell number. (b–f) Plots of spheroid size versus cell number for A549 (b), MDA-MB-231 (c), Min6 (d), L929 (e), and TTF (f). Data are expressed as mean±standard deviation (SD), *n*=6. (g) Brightfield images of CNF-induced spheroid formation at 48 h with increasing cell numbers.

4 Conclusions

In this study, we developed a nanofibril-driven technology for multi-cell spheroid formation as a strategy of CMDO. This nanofibril-integrated technology effectively promoted cell aggregation into a well-organized unit that enhanced the physiological structure and biological function. This approach was

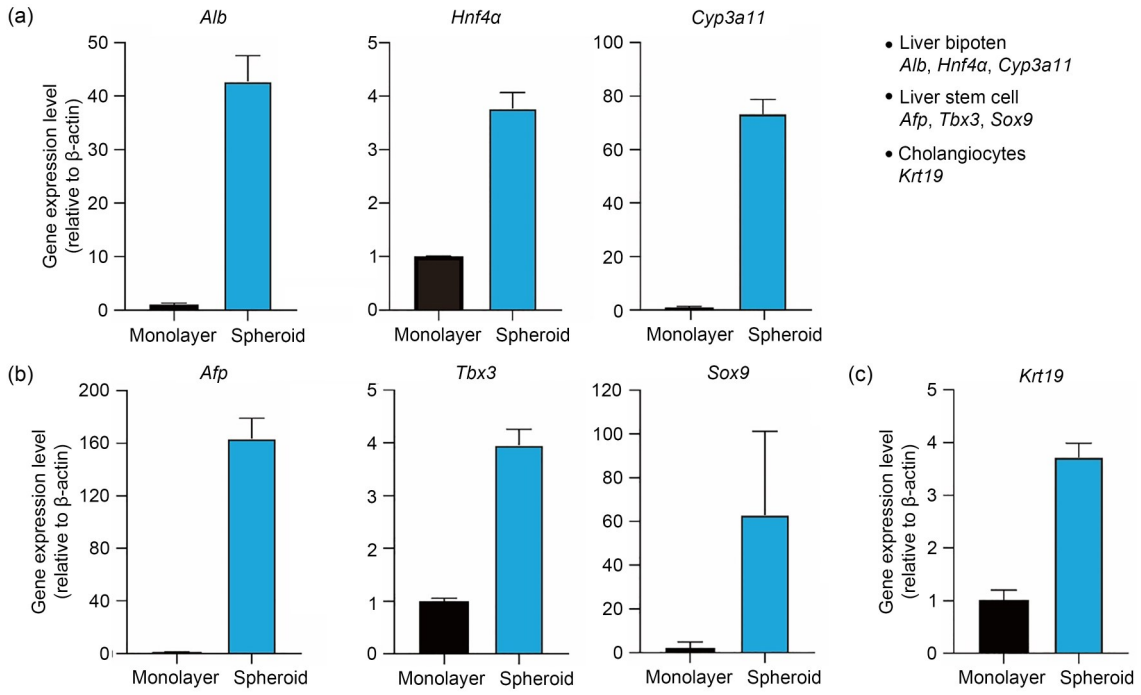

Fig. 6 Comparison of liver function-related gene profiles between monolayer cells and spheroids (monolayer culture is represented by the standard collagen dish coating culture method). (a) Hepatocyte markers: *Alb*, *Hnf4α*, and *Cyp3a11*; (b) Liver stem cell markers: *Afp*, *Tbx3*, and *Sox9*; (c) Cholangiocyte marker: *Krt19*. Data are expressed as mean± standard deviation (SD), *n*=3. *Alb*: albumin; *Hnf4α*: hepatocyte nuclear factor 4 α; *Cyp3a11*: cytochrome P450, family 3, subfamily A, polypeptide 11; *Afp*: alpha fetoprotein; *Tbx3*: T-box transcription factor 3; *Sox9*: sex-determining region Y-box 9; *Krt19*: keratin 19.

demonstrated as practical and reproducible, and validated using various cell types. In addition, CNF-based CMDOs were shown to facilitate spatiotemporal support for spheroid or tumoroid formation.

Data availability statement

All data generated or analyzed during this study are included in this published article. For further detailed information, please refer to Yuan YAO (yyao1@zju.edu.cn).

Acknowledgments

This work was supported by the National Natural Science Foundation of China (No. 32071347), the ZJU-Hangzhou Global Scientific and Technological Innovation Center, Zhejiang University (No. 02020200-K02013008), the Joint Laboratory Grant from Jiangsu Wuzhong Aesthetics Biotech Co., Ltd., and the Starting Grant of ShanghaiTech University. We also would like to thank the iBiofoundary and Core Facility of Institute for Intelligent Bio/Chem Manufacturing, Hangzhou Global Scientific and Technological Innovation Center (China) for fabrication and analysis.

Author contributions

Yuan YAO performed the following parts of this project: conceptualization, methodology, validation, investigation, writing – original draft, visualization, project administration, and funding acquisition. Yi LU and Guo LI completed the methodology, investigation, data organization, and manuscript writing. Guo LI organized the data and manuscript validation and investigation with the assist of Yeqiu LI. All authors have read and approved the final manuscript, and therefore, have full access to all the data in the study and take responsibility for the integrity and security of the data.

Compliance with ethics guidelines

Yi LU, Guo LI, Yeqiu LI, and Yuan YAO declare that they have no conflict of interest.

This paper does not contain any studies with human subjects performed by any of the authors. Cell lines were obtained from the Second Affiliated Hospital of Nanchang University (China) under the ethic regulation (No. BR/AF/SG-04/1.0).

References

Abdul Khalil HPS, Davoudpour Y, Islam MN, et al., 2014. Production and modification of nanofibrillated cellulose using various mechanical processes: a review. *Carbohydr Polym*, 99:649-665. https://doi.org/10.1016/j.carbpol.2013.08.069

Abouzeid RE, Khiari R, Beneventi D, et al., 2018. Biomimetic mineralization of three-dimensional printed alginate/TEMPO-oxidized cellulose nanofibril scaffolds for bone

tissue engineering. *Biomacromolecules*, 19(11):4442-4452. https://doi.org/10.1021/acs.biomac.8b01325

Alegret N, Dominguez-Alfaro A, Mecerreyes D, 2019. 3D scaffolds based on conductive polymers for biomedical applications. *Biomacromolecules*, 20(1):73-89. https://doi.org/10.1021/acs.biomac.8b01382

Al-Qararah AM, Ekman A, Hjelt T, et al., 2015. A unique microstructure of the fiber networks deposited from foam-fiber suspensions. *Colloids Surf A Physicochem Eng Aspects*, 482:544-553. https://doi.org/10.1016/j.colsurfa.2015.07.010

Amaral AJR, Pasparakis G, 2016. Rapid formation of cell aggregates and spheroids induced by a "smart" boronic acid copolymer. *ACS Appl Mater Interfaces*, 8(35):22930-22941. https://doi.org/10.1021/acsami.6b07911

Aumailley M, 2013. The laminin family. *Cell Adh Migr*, 7(1): 48-55. https://doi.org/10.4161/cam.22826

Badea MA, Balas M, Hermenean A, et al., 2019. Influence of Matrigel on single-and multiple-spheroid cultures in breast cancer research. *SLAS Discov*, 24(5):563-578. https://doi.org/10.1177/2472555219834698

Bagley JA, Reumann D, Bian S, et al., 2017. Fused cerebral organoids model interactions between brain regions. *Nat Methods*, 14(7):743-751. https://doi.org/10.1038/nmeth.4304

Bergmann S, Lawler SE, Qu Y, et al., 2018. Blood-brain-barrier organoids for investigating the permeability of CNS therapeutics. *Nat Protoc*, 13(12):2827-2843. https://doi.org/10.1038/s41596-018-0066-x

Broutier L, Mastrogiovanni G, Verstegen MMA, et al., 2017. Human primary liver cancer-derived organoid cultures for disease modeling and drug screening. *Nat Med*, 23(12): 1424-1435. https://doi.org/10.1038/nm.4438

Bryant KL, Stalnecker CA, Zeitouni D, et al., 2019. Combination of ERK and autophagy inhibition as a treatment approach for pancreatic cancer. *Nat Med*, 25(4):628-640. https://doi.org/10.1038/s41591-019-0368-8

Buchroithner B, Klausegger A, Ebschner U, et al., 2004. Analysis of the *LAMB3* gene in a junctional epidermolysis bullosa patient reveals exonic splicing and allele-specific nonsense-mediated mRNA decay. *Lab Invest*, 84(10):1279-1288. https://doi.org/10.1038/labinvest.3700164

Chen J, Zhang JT, Yang L, et al., 2023. Facile suspension culture protocol of the liver biliary organoids. *Bio-Des Manuf*, 6(1):74-81. https://doi.org/10.1007/s42242-022-00213-3

Chen YW, Huang SX, de Carvalho ALRT, et al., 2017. A three-dimensional model of human lung development and disease from pluripotent stem cells. *Nat Cell Biol*, 19(5): 542-549. https://doi.org/10.1038/ncb3510

Chung H, Jung H, Lee JH, et al., 2014. Keratinocyte-derived laminin-332 protein promotes melanin synthesis via regulation of tyrosine uptake. *J Biol Chem*, 289(31):21751-21759. https://doi.org/10.1074/jbc.M113.541177

Cruz NM, Song XW, Czerniecki SM, et al., 2017. Organoid cystogenesis reveals a critical role of microenvironment in human polycystic kidney disease. *Nat Mater*, 16(11): 1112-1119. https://doi.org/10.1038/nmat4994

Curvello R, Kerr G, Micati DJ, et al., 2021. Engineered plant-based nanocellulose hydrogel for small intestinal organoid growth. *Adv Sci*, 8(1):2002135. https://doi.org/10.1002/advs.202002135

Davies JA, 2013. The power and limitations of self-assembly. *In*: Davies JA (Ed.), Mechanisms of Morphogenesis, 2nd Ed. Academic Press, Waltham, p.17-30. https://doi.org/10.1016/B978-0-12-391062-2.00003-6

di Martino JS, Nobre AR, Mondal C, et al., 2022. A tumor-derived type III collagen-rich ECM niche regulates tumor cell dormancy. *Nat Cancer*, 3(1):90-107. https://doi.org/10.1038/s43018-021-00291-9

Drost J, Clevers H, 2018. Organoids in cancer research. *Nat Rev Cancer*, 18(7):407-418. https://doi.org/10.1038/s41568-018-0007-6

Edelman GM, 1983. Cell adhesion molecules. *Science*, 219(4584): 450-457. https://doi.org/10.1126/science.6823544

Evdokimova OL, Alves CS, Krsmanović Whiffen RM, et al., 2021. Cytocompatible cellulose nanofibers from invasive plant species *Agave americana* L. and *Ricinus communis* L.: a renewable green source of highly crystalline nanocellulose. *J Zhejiang Univ-Sci B (Biomed & Biotechnol)*, 22(6):450-461. https://doi.org/10.1631/jzus.B2000683

Fang M, Goldstein EL, Matich EK, et al., 2013. Type I collagen self-assembly: the roles of substrate and concentration. *Langmuir*, 29(7):2330-2338. https://doi.org/10.1021/la3048104

Ferreira FV, Otoni CG, de France KJ, et al., 2020. Porous nanocellulose gels and foams: breakthrough status in the development of scaffolds for tissue engineering. *Mater Today*, 37:126-141. https://doi.org/10.1016/j.mattod.2020.03.003

Fitsialos G, Bourget I, Augier S, et al., 2008. HIF1 transcription factor regulates laminin-332 expression and keratinocyte migration. *J Cell Sci*, 121(Pt 18):2992-3001. https://doi.org/10.1242/jcs.029256

Fujii M, Shimokawa M, Date S, et al., 2016. A colorectal tumor organoid library demonstrates progressive loss of niche factor requirements during tumorigenesis. *Cell Stem Cell*, 18(6):827-838. https://doi.org/10.1016/j.stem.2016.04.003

Garreta E, Prado P, Tarantino C, et al., 2019. Fine tuning the extracellular environment accelerates the derivation of kidney organoids from human pluripotent stem cells. *Nat Mater*, 18(4):397-405. https://doi.org/10.1038/s41563-019-0287-6

Goetz JG, Minguet S, Navarro-Lérida I, et al., 2011. Biomechanical remodeling of the microenvironment by stromal caveolin-1 favors tumor invasion and metastasis. *Cell*, 146(1):148-163.

https://doi.org/10.1016/j.cell.2011.05.040

Gonzalez-Rodriguez D, Guevorkian K, Douezan S, et al., 2012. Soft matter models of developing tissues and tumors. *Science*, 338(6109):910-917. https://doi.org/10.1126/science.1226418

Grassi L, Alfonsi R, Francescangeli F, et al., 2019. Organoids as a new model for improving regenerative medicine and cancer personalized therapy in renal diseases. *Cell Death Dis*, 10(3):201. https://doi.org/10.1038/s41419-019-1453-0

Hale LJ, Howden SE, Phipson B, et al., 2018. 3D organoid-derived human glomeruli for personalised podocyte disease modelling and drug screening. *Nat Commun*, 9:5167. https://doi.org/10.1038/s41467-018-07594-z

Hegedüs B, Marga F, Jakab K, et al., 2006. The interplay of cell-cell and cell-matrix interactions in the invasive properties of brain tumors. *Biophys J*, 91(7):2708-2716. https://doi.org/10.1529/biophysj.105.077834

Holmes DF, Lu YH, Starborg T, et al., 2018. Collagen fibril assembly and function. *Curr Top Dev Biol*, 130:107-142. https://doi.org/10.1016/bs.ctdb.2018.02.004

Homan KA, Gupta N, Kroll KT, et al., 2019. Flow-enhanced vascularization and maturation of kidney organoids in vitro. *Nat Methods*, 16(3):255-262. https://doi.org/10.1038/s41592-019-0325-y

Hu KS, Kulkarni DD, Choi I, et al., 2014. Graphene-polymer nanocomposites for structural and functional applications. *Prog Polym Sci*, 39(11):1934-1972. https://doi.org/10.1016/j.progpolymsci.2014.03.001

Huang C, Dai JX, Zhang XA, 2015. Environmental physical cues determine the lineage specification of mesenchymal stem cells. *Biochim Biophys Acta (BBA)-Gen Subj*, 1850(6):1261-1266. https://doi.org/10.1016/j.bbagen.2015.02.011

Jadin KD, Wong BL, Bae WC, et al., 2005. Depth-varying density and organization of chondrocytes in immature and mature bovine articular cartilage assessed by 3D imaging and analysis. *J Histochem Cytochem*, 53(9):1109-1119. https://doi.org/10.1369/jhc.4A6511.2005

Jaeckel S, Kaller M, Jackstadt R, et al., 2018. *Ap4* is rate limiting for intestinal tumor formation by controlling the homeostasis of intestinal stem cells. *Nat Commun*, 9:3573. https://doi.org/10.1038/s41467-018-06001-x

Jager M, Blokzijl F, Sasselli V, et al., 2018. Measuring mutation accumulation in single human adult stem cells by whole-genome sequencing of organoid cultures. *Nat Protoc*, 13(1):59-78. https://doi.org/10.1038/nprot.2017.111

Jung SN, Lim HS, Liu LH, et al., 2018. LAMB3 mediates metastatic tumor behavior in papillary thyroid cancer by regulating c-MET/Akt signals. *Sci Rep*, 8:2718. https://doi.org/10.1038/s41598-018-21216-0

Karageorgiou V, Kaplan D, 2005. Porosity of 3D biomaterial scaffolds and osteogenesis. *Biomaterials*, 26(27):5474-5491. https://doi.org/10.1016/j.biomaterials.2005.02.002

Karzbrun E, Kshirsagar A, Cohen SR, et al., 2018. Human brain organoids on a chip reveal the physics of folding. *Nat Phys*, 14(5):515-522. https://doi.org/10.1038/s41567-018-0046-7

Katsuda T, Kawamata M, Hagiwara K, et al., 2017. Conversion of terminally committed hepatocytes to culturable bipotent progenitor cells with regenerative capacity. *Cell Stem Cell*, 20(1):41-55. https://doi.org/10.1016/j.stem.2016.10.007

Kobayashi Y, Saito T, Isogai A, 2014. Aerogels with 3D ordered nanofiber skeletons of liquid-crystalline nanocellulose derivatives as tough and transparent insulators. *Angew Chem Int Ed*, 53(39):10394-10397. https://doi.org/10.1002/anie.201405123

Kronenberg HM, 2003. Developmental regulation of the growth plate. *Nature*, 423(6937):332-336. https://doi.org/10.1038/nature01657

Krüger M, Oosterhoff LA, van Wolferen ME, et al., 2020. Cellulose nanofibril hydrogel promotes hepatic differentiation of human liver organoids. *Adv Healthc Mater*, 9(6):1901658. https://doi.org/10.1002/adhm.201901658

Landry MJ, Rollet FG, Kennedy TE, et al., 2018. Layers and multilayers of self-assembled polymers: tunable engineered extracellular matrix coatings for neural cell growth. *Langmuir*, 34(30):8709-8730. https://doi.org/10.1021/acs.langmuir.7b04108

Lawlor KT, Vanslambrouck JM, Higgins JW, et al., 2021. Cellular extrusion bioprinting improves kidney organoid reproducibility and conformation. *Nat Mater*, 20(2):260-271. https://doi.org/10.1038/s41563-020-00853-9

Li JW, Wu MX, Chen WH, et al., 2021. 3D printing of bioinspired compartmentalized capsular structure for controlled drug release. *J Zhejiang Univ-Sci B (Biomed & Biotechnol)*, 22(12):1022-1033. https://doi.org/10.1631/jzus.B2100644

Louis F, Pannetier P, Souguir Z, et al., 2017. A biomimetic hydrogel functionalized with adipose ECM components as a microenvironment for the 3D culture of human and murine adipocytes. *Biotechnol Bioeng*, 114(8):1813-1824. https://doi.org/10.1002/bit.26306

Malafaya PB, Silva GA, Reis RL, 2007. Natural-origin polymers as carriers and scaffolds for biomolecules and cell delivery in tissue engineering applications. *Adv Drug Deliv Rev*, 59(4-5):207-233. https://doi.org/10.1016/j.addr.2007.03.012

Martinez-Vidal L, Murdica V, Venegoni C, et al., 2021. Causal contributors to tissue stiffness and clinical relevance in urology. *Commun Biol*, 4:1011. https://doi.org/10.1038/s42003-021-02539-7

Martoïa F, Cochereau T, Dumont PJJ, et al., 2016. Cellulose nanofibril foams: links between ice-templating conditions, microstructures and mechanical properties. *Mater Des*, 104:376-391. https://doi.org/10.1016/j.matdes.2016.04.088

Miller AJ, Dye BR, Ferrer-Torres D, et al., 2019. Generation of lung organoids from human pluripotent stem cells in vitro. *Nat Protoc*, 14(2):518-540. https://doi.org/10.1038/s41596-018-0104-8

Miner JH, Yurchenco PD, 2004. Laminin functions in tissue morphogenesis. *Annu Rev Cell Dev Biol*, 20:255-284.

https://doi.org/10.1146/annurev.cellbio.20.010403.094555

Mittal N, Ansari F, Gowda VK, et al., 2018. Multiscale control of nanocellulose assembly: transferring remarkable nanoscale fibril mechanics to macroscale fibers. *ACS Nano*, 12(7):6378-6388. https://doi.org/10.1021/acsnano.8b01084

Mohan N, Gupta V, Sridharan B, et al., 2014. The potential of encapsulating "raw materials" in 3D osteochondral gradient scaffolds. *Biotechnol Bioeng*, 111(4):829-841. https://doi.org/10.1002/bit.25145

Mouw JK, Ou GQ, Weaver VM, 2014. Extracellular matrix assembly: a multiscale deconstruction. *Nat Rev Mol Cell Biol*, 15(12):771-785. https://doi.org/10.1038/nrm3902

Mueller M, Rasoulinejad S, Garg S, et al., 2020. The importance of cell-cell interaction dynamics in bottom-up tissue engineering: concepts of colloidal self-assembly in the fabrication of multicellular architectures. *Nano Lett*, 20(4): 2257-2263. https://doi.org/10.1021/acs.nanolett.9b04160

Nechyporchuk O, Belgacem MN, Pignon F, 2016a. Current progress in rheology of cellulose nanofibril suspensions. *Biomacromolecules*, 17(7):2311-2320. https://doi.org/10.1021/acs.biomac.6b00668

Nechyporchuk O, Belgacem MN, Bras J, 2016b. Production of cellulose nanofibrils: a review of recent advances. *Ind Crops Prod*, 93:2-25. https://doi.org/10.1016/j.indcrop.2016.02.016

Nguyen NM, Senior RM, 2006. Laminin isoforms and lung development: all isoforms are not equal. *Dev Biol*, 294(2): 271-279. https://doi.org/10.1016/j.ydbio.2006.03.032

Ortega-Prieto AM, Skelton JK, Wai SN, et al., 2018. 3D microfluidic liver cultures as a physiological preclinical tool for hepatitis B virus infection. *Nat Commun*, 9:682. https://doi.org/10.1038/s41467-018-02969-8

Park D, Wershof E, Boeing S, et al., 2020. Extracellular matrix anisotropy is determined by TFAP2C-dependent regulation of cell collisions. *Nat Mater*, 19(2):227-238. https://doi.org/10.1038/s41563-019-0504-3

Park M, Lee D, Shin S, et al., 2015. Effect of negatively charged cellulose nanofibers on the dispersion of hydroxyapatite nanoparticles for scaffolds in bone tissue engineering. *Colloids Surf B Biointerfaces*, 130:222-228. https://doi.org/10.1016/j.colsurfb.2015.04.014

Phipson B, Er PX, Combes AN, et al., 2019. Evaluation of variability in human kidney organoids. *Nat Methods*, 16(1): 79-87. https://doi.org/10.1038/s41592-018-0253-2

Qian XY, Jacob F, Song MM, et al., 2018. Generation of human brain region-specific organoids using a miniaturized spinning bioreactor. *Nat Protoc*, 13(3):565-580. https://doi.org/10.1038/nprot.2017.152

Rasoulinejad S, Mueller M, Nzigou Mombo B, et al., 2020. Orthogonal blue and red light controlled cell–cell adhesions enable sorting-out in multicellular structures. *ACS Synth Biol*, 9(8):2076-2086. https://doi.org/10.1021/acssynbio.0c00150

Reid MS, Villalobos M, Cranston ED, 2017. Benchmarking cellulose nanocrystals: from the laboratory to industrial production. *Langmuir*, 33(7):1583-1598. https://doi.org/10.1021/acs.langmuir.6b03765

Ren J, Wang Y, Yao Y, et al., 2019. Biological material interfaces as inspiration for mechanical and optical material designs. *Chem Rev*, 119(24):12279-12336. https://doi.org/10.1021/acs.chemrev.9b00416

Ren X, Wang FY, Chen C, et al., 2016. Engineering zonal cartilage through bioprinting collagen type II hydrogel constructs with biomimetic chondrocyte density gradient. *BMC Musculoskelet Disord*, 17:301. https://doi.org/10.1186/s12891-016-1130-8

Robins SP, 2006. Fibrillogenesis and maturation of collagens. *In*: Seibel MJ, Robins SP, Bilezikian JP (Eds.), Dynamics of Bone and Cartilage Metabolism, 2nd Ed. Academic Press, San Diego, p.41-53. https://doi.org/10.1016/B978-012088562-6/50003-0

Roerink SF, Sasaki N, Lee-Six H, et al., 2018. Intra-tumour diversification in colorectal cancer at the single-cell level. *Nature*, 556(7702):457-462. https://doi.org/10.1038/s41586-018-0024-3

Rohn F, Kordes C, Castoldi M, et al., 2018. Laminin-521 promotes quiescence in isolated stellate cells from rat liver. *Biomaterials*, 180:36-51. https://doi.org/10.1016/j.biomaterials.2018.07.008

Roi A, Ardelean LC, Roi CI, et al., 2019. Oral bone tissue engineering: advanced biomaterials for cell adhesion, proliferation and differentiation. *Materials (Basel)*, 12(14):2296. https://doi.org/10.3390/ma12142296

Rossi G, Manfrin A, Lutolf MP, 2018. Progress and potential in organoid research. *Nat Rev Genet*, 19(11):671-687. https://doi.org/10.1038/s41576-018-0051-9

Saito Y, Muramatsu T, Kanai Y, et al., 2019. Establishment of patient-derived organoids and drug screening for biliary tract carcinoma. *Cell Rep*, 27(4):1265-1276.e4. https://doi.org/10.1016/j.celrep.2019.03.088

Steinberg MS, 1962. On the mechanism of tissue reconstruction by dissociated cells, III. Free energy relations and the reorganization of fused, heteronomic tissue fragments. *Proc Natl Acad Sci USA*, 48(10):1769-1776. https://doi.org/10.1073/pnas.48.10.1769

Sun T, Norton D, McKean RJ, et al., 2007. Development of a 3D cell culture system for investigating cell interactions with electrospun fibers. *Biotechnol Bioeng*, 97(5):1318-1328. https://doi.org/10.1002/bit.21309

Tevis KM, Colson YL, Grinstaff MW, 2017. Embedded spheroids as models of the cancer microenvironment. *Adv Biosyst*, 1(10):1700083. https://doi.org/10.1002/adbi.20170008

Thunberg J, Kalogeropoulos T, Kuzmenko V, et al., 2015. In situ synthesis of conductive polypyrrole on electrospun cellulose nanofibers: scaffold for neural tissue engineering. *Cellulose*, 22(3):1459-1467. https://doi.org/10.1007/s10570-015-0591-5

Tuveson D, Clevers H, 2019. Cancer modeling meets human organoid technology. *Science*, 364(6444):952-955.

https://doi.org/10.1126/science.aaw6985

Winkler S, Kaplan DL, 2001. Biosynthesized materials: properties and processing. *In*: Buschow KHJ, Cahn RW, Flemings MC, et al. (Eds.), Encyclopedia of Materials: Science and Technology, 2nd Ed. Elsevier, Amsterdam, p.609-615. https://doi.org/10.1016/B0-08-043152-6/00117-0

Xiao RR, Jin L, Xie N, et al., 2022. Establishment and large-scale validation of a three-dimensional tumor model on an array chip for anticancer drug evaluation. *Front Pharmacol*, 13:1032975. https://doi.org/10.3389/fphar.2022.1032975

Yang X, Reid MS, Olsén P, et al., 2020. Eco-friendly cellulose nanofibrils designed by nature: effects from preserving native state. *ACS Nano*, 14(1):724-735. https://doi.org/10.1021/acsnano.9b07659

Yeatts AB, Choquette DT, Fisher JP, 2013. Bioreactors to influence stem cell fate: augmentation of mesenchymal stem cell signaling pathways via dynamic culture systems. *Biochim Biophys Acta (BBA)-Gen Subj*, 1830(2):2470-2480. https://doi.org/10.1016/j.bbagen.2012.06.007

Zhang XF, Xiong R, Kang S, et al., 2020. Alternating stacking of nanocrystals and nanofibers into ultrastrong chiral biocomposite laminates. *ACS Nano*, 14(11):14675-14685. https://doi.org/10.1021/acsnano.0c06192

Zhu ZH, Song JL, Guo YG, et al., 2020. LAMB3 promotes tumour progression through the AKT-FOXO3/4 axis and is transcriptionally regulated by the BRD2/acetylated ELK4 complex in colorectal cancer. *Oncogene*, 39(24):4666-4680. https://doi.org/10.1038/s41388-020-1321-5

Supplementary information

Figs. S1–S7